Extending the Range of Rupture Force Measurements with Axial Optical Tweezers

Z. Zhang[1,2] and J. N. Milstein[1,2,*]

[1] *University of Toronto, Department of Physics, Toronto, Ontario, Canada*

[2] *University of Toronto Mississauga,*

Department of Chemical and Physical Sciences, Mississauga, Ontario, Canada

Abstract

Axial force-spectroscopy with optical tweezers provides a natural geometry for performing rupture force measurements of protein and nucleic acid binding interactions. Axial traps, however, are typically weaker than their lateral counterparts requiring a high laser power to maintain a well calibrated, linear restoring force. Moreover, at higher forces, unless the surface tethering is carefully designed, various linkages involved in the tethering may rupture before the actual system of interest. Here we show how rupture force measurements on surface tethered molecules, up to a maximum force of ~ 45 pN, may be designed and performed with axial optical tweezers. As both a proof of principle and a study in designing a protein handle, we explore the rupture forces involved in detaching ssDNA oligomers of varying lengths from a tethered DNA substrate. We find that the presence of short stretches of ssDNA, between the bound oligomer and substrate DNA, can significantly stabilize the binding interaction under an applied force.

*Electronic address: `josh.milstein@utoronto.ca`

I. INTRODUCTION

Optical tweezers remain one of the most precise techniques for measuring forces involved in the interactions between biological molecules [1]. Compared to other single-molecule force-spectroscopic techniques, such as atomic-force microscopy (AFM) or magnetic tweezers, optical tweezers provide access to the sub-piconewton to piconewton force regime with higher resolution and sensitivity, which is essential for characterizing many protein/nucleic acid interactions [2]. One common application is to vary the loading rate on a bound biomolecular system, typically through a linear ramp, to measure rate-dependent unbinding forces. These dynamic force measurements can be used to characterize the energy landscape of a biomolecular interaction yielding parameters such as the kinetic constants (k_{on}, k_{off}), binding affinity (K_d), and energy (ΔG) and distance (Δx) to the transition state [3, 4].

Axial optical tweezers, which apply forces perpendicular to surface tethered molecules (i.e., along the laser axis), may have certain advantages over more conventional trapping geometries [5]. Axial tweezers allow for the use of short tethers, which greatly reduces the compliance of the system and can significantly increase the signal-to-noise of a measurement. And compared to conventional dumbbell tweezers [2], the throughput is much better as measurements can be quickly repeated on untouched, tethered molecules. While an axial geometry seems straightforward enough, challenges in calibrating this technique, primarily due to the fact that the trap strength varies as it is translated and that one needs to precisely measure the trapped bead's distance from the coverslip surface, have limited its adoption by the biophysical community. However, in recent years, these challenges have largely been overcome [5].

In this manuscript, we describe how axial tweezers can provide a convenient method for measuring rupture forces as large as $\sim$ 45 pN with DNA tethers. At these forces, many of the linkages utilized in standard approaches to surface tethering fail. And without employing high laser powers, at $\sim$ 10s of piconewtons it becomes increasingly difficult to maintain an axial trap stiff enough to prevent errors in the force calibration. We have systematically studied both the challenges in using DNA as a tether as well as the calibration corrections required to perform axial rupture force measurements of up to $\sim$ 45 pN. To illustrate the resulting technique, with an eye toward optimizing the design of a protein handle, we have systematically explored the rupture forces involved in peeling ssDNA oligomers of varying

lengths from a tethered DNA substrate. Our results provide the reader with a practical assay for designing and performing rupture force measurements with axial optical tweezers.

II. MATERIALS AND METHODS

A. Optical tweezers setup

The axial tweezers setup employs a standard configuration for a single-beam optical tweezers (see *Supplementary Material*). A Nd:YAG laser (Spectra Physics, 1064nm, BL-106C), used for optical trapping, is first passed through an optical isolator then circularized by passage through a pin-hole. Two sets of telescopes adjust the beam size at the back aperture of the objective (Olympus PLAPON 60XO, 60x, oil-immersion, N.A.=1.42) to $\sim$ 11 mm (full width at $1/e^2$ intensity), matching the size of the back aperture (11 mm) to form a strong axial optical trap. A second objective (Olympus UPLFLN40X, 40x, N.A.=0.75) is used as a condenser to collect the laser light with its back focal plane conjugated by an additional lens onto a position sensitive diode (PSD, First Sensor, DL100-7-PCBA3). We used a red LED to illuminate the sample for bright field imaging with a CMOS camera (Pixielink PL-B781F). The sample chamber was translated axially along the laser axis by a piezo-stage (Mad City Labs, Nano-LP100). All data was acquired via LabView and and processed by custom MatLab scripts.

B. Surface functionalization

Coverslips were first sonicated in isoproponal for 10 min, followed by a rinse with deionized water, then sonicated in deionized water for 10 min. Washed coverslips were blown dry with medical grade compressed air then plasma-cleaned for 2 min. Three common surface functionalization methods were tested for tethering to a coverslip:

1. Nitrocellulose w/ streptavidin: We used a protocol similar to [6]. Nitrocellulose solution (4-8% in ethanol/diethyl ether, Sigma-Aldrich, 09986) was diluted to $\sim$ 0.2% with amyl acetate (Sigma-Aldrich, W454009). Immediately after plasma-cleaning, coverslips were immersed in diluted nitrocellulose solution for 5 s, then dried by absorbing excessive solution with a Kimwipe at one end of the coverslip, then dried in vacuum overnight. After

drying, a flow chamber was made from sandwiching two thin, parallel strips of parafilm between two coverslips and heating to 85°C. Then 0.5 mg/mL streptavidin (Promega, Z7041, dissolved in PBS buffer, pH 7.4) was flowed into the chamber and incubated for 1h, followed by 100 mg/mL BSA (Sigma-Aldrich, A7906, dissolved in PBS buffer, pH 7.4) incubated for another 30 min to passivate the surface. Finally, the chamber was washed with PBS buffer.

2. Hydrophilic w/ BSA-biotin and streptavidin: After plasma cleaning, the overslip surface is hydrophilic because of the oxidation and formation of hydroxyl groups. Immediately after plasma-cleaning, the coverslips were stored in deionized water and dried with compressed air before use. Flow chamber were made as previously described, then 1 mg/mL BSA-Biotin (Sigma-Aldrich, A8549, dissolved in PBS buffer, pH 7.4) was first flowed in and incubated for 10 min, followed by 100 mg/mL BSA (Sigma-Aldrich, A7906, dissolved in PBS buffer, pH 7.4) for another 10 min incubation to passivate the surface. After a thorough washing with at least 10x the chamber volume of PBS, 0.5 mg/mL streptavidin (in PBS) was flowed in and incubated for 10 min. A final wash step with PBS buffer was performed after incubation.

3. Nitrocellulose or hydrophilic w/ anti-DIG: Protocols are similar to those for attaching streptavidin to the surface. When using nitrocellulose, replace streptavidin with 20 ug/mL anti-DIG (Roche, 11333089001, dissolved in PBS buffer, pH 7.4) and incubate for 30 min. When using a hydrophilic surface, replace BSA-biotin with 20 ug/mL anti-DIG and incubate for 30 min. Always passivate by flowing in 100 mg/mL BSA and incubate for 10 min. Wash with PBS buffer after incubation.

Although a nitrocellulose coated surface, 1, is often employed when applying high forces to tethered DNA, we found that coating a hydrophobic surface with streptavidin, 2, to be the most resistant to rupture. Likewise, this approach also tended to yield a rather flat level of background to the rupture force distributions. Replacing the streptavidin-biotin linkage with a digoxigenin-antidigoxigenin introduced a significant amount of noise in the data as a significant portion of the ruptures by the antibody/antigen linkage occur below 45 pN (see *Supplementary Material*).

C. DNA tether assembly

All DNA constructs used in this research were synthesized by two rounds of PCR. In the first round, lambda-DNA was used as a template. The following forward [GCT ACG GAT TCA TAG ACT GCT GGG AAC TCC GGG TGC TAT CAG] and reverse [CAG CGT CAC AAC AAT CAG CC] primers were employed throughout. In the forward primer, the first 22 nucleotides complement a 5' biotin or digoxigenin modified primer in the second round, and the remaining 20 nucleotides complement the lambda-DNA template. This enables us to change the length of the tether by varying this simple primer, but without having to purchase multiple 5' modified primers. With these two primers, we sythesized linear dsDNA with a contour length of 4598 bps.

For the second round of PCR, the product of the first PCR was used as a template. We employed the following two primers: forward [(overhang)-(abasic site)-CAG CGT CAC AAC AAT CAG CC] and reverse [Bio/Dig-GCT ACG GAT TCA TAG ACT GCT G]. DNA produced in this round will have either biotin (Bio) or digoxigenin (Dig) at one end for surface attachment. At the other end, the introduction of an abasic site results in an ssDNA overhang of varying length and defined sequence (overhang).

The resulting partial tethers are diluted to $\sim$ 10 pM and pipetted into passivated, surface functionalized flow chambers and incubated for 10 min. For streptavidin coated surfaces, 10 μM biotin (BioShop, BIO302.1, dissolved in PBS buffer, pH 7.4) is flowed in and incubated for 10 min to block binding between surface bound streptavidin and the biotin-modified oligos in the next step. The chamber is then washed with PBS. Complementary biotin/DIG modified oligos are then flowed into the chambers and allowed to anneal to the surface tethered DNA for 15 min. Finally, wash with PBS, flow in streptavidin/anti-DIG coated beads, and wait for at least 10 min before an experiment.

All sequences for the various overhangs and complementary oligos are provided in the *Supplementary Material*.

D. Axial force calibration

In this manuscript, we follow a procedure adapted from Mack et al. [7]. In brief, axial tweezers require a calibration for both the sensitivity and the trap strength at varying heights

above the coverslip surface. This may be obtained by trapping a free bead, within a fixed trap, and varying the height by a vertical displacement of the stage. At each axial position, both the sensitivity and trap strength may be extracted from an analysis of the resulting power spectrum. The displacement of the bead from the trap center can then be obtained by comparing the intensity to the intensity of a free bead within the optical trap at that height. However, we still need to know the position of the trap center. As Mack et al. showed, this can be inferred from the backscattering of light between the trapped bead and the coverslip surface, which gives rise to an oscillatory signal as the trap is translated axially (see [5, 7] for details).

Instead of performing these calibrations in advance, in our rupture force measurements, we extend each construct by displacing the stage while recording the intensity until a rupture event occurs. We then scan the now 'free' bead back toward the surface recording the sensitivity and trap strength at each height and using the resulting intensity scan to calibrate for the trap position. This approach is more robust than a single calibration step since sample drift can be accounted for by aligning the backward scan with the initial, low-force portion of the forward scan.

III. RESULTS

A. Laser power and the range of applied forces

Surface tethered dsDNA is a convenient handle for single-molecule force measurements as both the 3' and 5' ends can be easily functionalized for attachment [8]. Likewise, its elastic properties are well characterised and may be directly accounted for when extracting lifetimes from dynamic rupture force measurements [3]. When stretched, dsDNA initially behaves as a linear spring, but at increasing force the intrinsic elasticity of the polymer must be incorporated [9, 10]. Under typical buffer conditions, the worm-like chain (WLC) model holds up to $\sim 10-15$ pN after which the response is essentially linear and may be described by the extensible worm-like chain (eWLC) up to ~ 45 pN. Below this threshold, dsDNA remains in its B-form, but then the response curve begins to flatten and at $\sim 60-65$ pN dsDNA begins to overstretch. The overstretching transition is stochastic at standard salt concentrations and, essentially, sets an upper limit to the range of applied forces over which

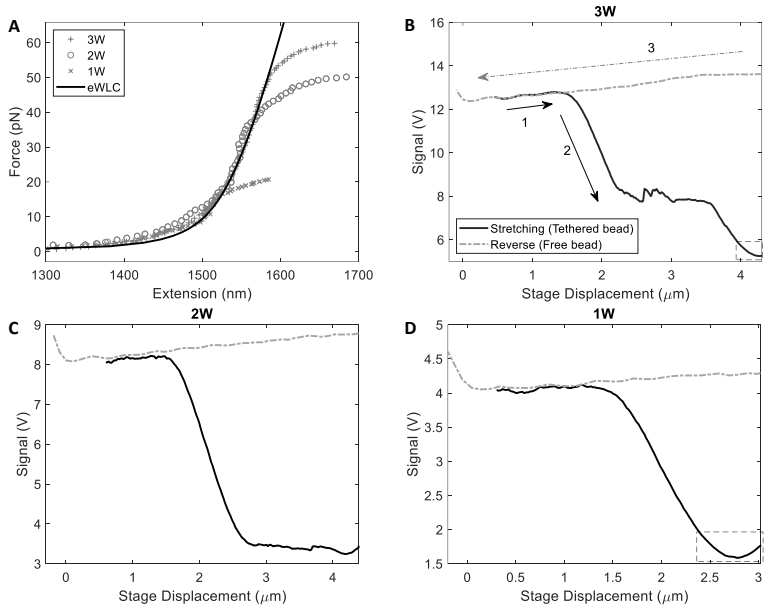

FIG. 1: A) Axial force-extension curves acquired at 1 W, 2 W, and 3 W of laser power. Measurements taken at less than 3 W appear to approach the overstretching transition at lower applied forces. A fit to the eWLC is shown (solid line). B) Photodiode signal vs stage position during a rupture force measurement at 3 W. A trapped and tethered bead is first pulled away from the surface by moving the stage. Initially, the bead moves with the trap (1), but then the effects of the tether become apparent and the DNA responds like an eWLC, eventually, overstretching (2). In this example, the DNA was stretched far enough that we could observe it exit the overstretching regime and again display a relatively linear restoring force before eventually rupturing. After rupture, the stage is moved back to its initial position, and the free bead signal is recorded as part of the calibration (3). Photodiode signal vs stage position at C) 2 W and D) 1 W . In both C and D, the nonlinear response of the trap is apparent during the force ramp (indicated by dashed boxes), but is difficult to detect in the flat region of the overstretching regime.

dsDNA is useful as a flexible linker.

Figure 1A displays a series of force-extension curves taken at laser powers ranging from 1-3 W (note, we indicate the power out of the laser which translates to $\approx$ 0.3 W, 0.6 W, and 0.9 W, respectively, at the trap). At both 2 W and 3 W, the overstretching regime is clearly visible, but at 2 W it appears to occur at a much lower applied force ($\sim$ 50 pN). At an even lower laser power of 1 W, the force-extension curve begins to flatten, deviating from the eWLC model at just $\sim$ 20 pN.

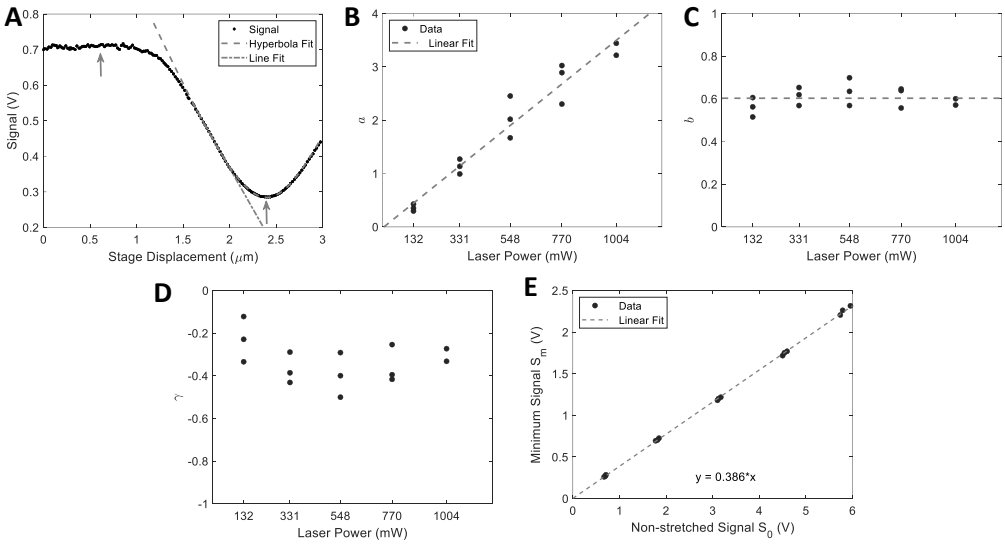

FIG. 2: Generalized calibration of of the detector signal to account for a non-linear response at higher forces. A) Example signal at 132 mW laser power when stretching DNA. Both a linear fit and a hyperbola fit, as explained in the text, are shown. The arrow on top indicates the effective "non-stretched" signal S_0 and bottom arrow points to the minimum signal S_m. B-D) Fitting parameters for hyperbola fit to signal at different laser powers. The dashed line in C indicates the mean of the data. E) Linear relation between the minimum signal S_m and and the non-stretched signal S_0.

Figures 1B-C help illuminate the origins of this behavior. Here we display the photodiode signal as a function of stage position. The solid lines each represent a dsDNA tethered bead held fixed by an optical trap as the stage is displaced vertically, and the dashed-dotted lines are the signal from that same bead, now untethered, as the stage is scanned back across the range. To translate these measurements into the force-extension curves shown in Fig. 1A, we assume that the applied force is linearly proportional to the displacement Δx of the bead from the trap center and that Δx is linearly proportional to the diode voltage. The proportionality constants are given by the spring constant k and sensitivity β, respectively, which were measured at each axial position. These calibration measurements, however, were made with a free bead well within the harmonic region of the trap where our assumptions of linearity clearly hold. However, upon forcible extension of the dsDNA, within an insufficiently strong trap, the bead may get pulled into a region of the trap where these linear relations break down.

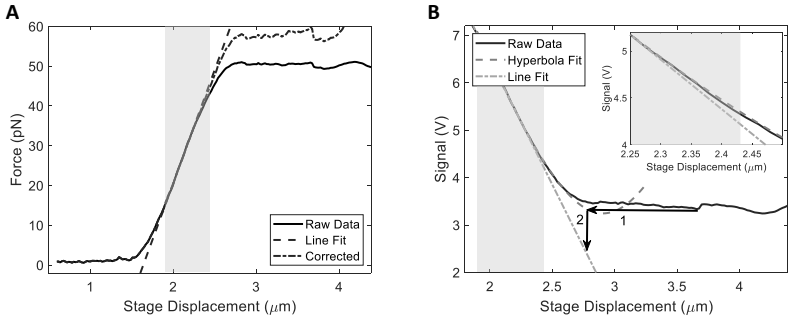

FIG. 3: Rescaling the measured signal to account for the nonlinear response at reduced laser power. A) Force vs stage displacement curves for the original measured signal (solid line) and the corrected signal (dashed-dotted line). The dashed line is a linear fit to the linear portion of the data. At 2 W, the force-displacement curves will deviate from this linear trend prematurely if the bead is pulled too far from the trap center. B) Plot of the signal vs. stage displacement. To correct the force-displacement curve, a hyberbola (dashed line) is first fit to the signal approximating the nonlinear response. The region of the fit is indicated by the shading and spans from x_l to $x_{45}*$ (the insert provides a magnified view of the fitted region). Each data point is first mapped to this hyperbola (arrow 1) then mapped to the linear extrapolation (arrow 2). The the effect of this rescaling (dashed-dotted line in A) is that the data collected at 2 W is now in agreement with that collected within a stiffer trap.

This nonlinear signal response can clearly be seen at low laser power (1 W, Fig. 1D). As the stage is moved progressively further, the signal becomes linear, in agreement with the eWLC, but is eventually observed to turn over. This same signature behavior is seen at high laser power (3 W, Fig. 1B) within the linear regime beyond the overstretching transition. However, when this nonlinear response in the signal occurs close to or within the overstretching regime, it is less obvious since the actual force required to extend the DNA tether is stochastic about a relatively constant value, which obscures the signature shape of the nonlinearity (Fig. 1C).

This observation seems to imply that, for our setup, we need approximately 3 W of laser power to reach the overstretching regime. Similarly, to make axial rupture force measurements up to 45 pN, or throughout the full range of the linear restoring force region, would

require around 3 W of laser power. A reduction in laser power would restrict the upper range of forces we may apply. However, the force-extension curves at both 3 W and 2 W appear qualitatively similar. The overstretching regime simply appears at too low an applied force when measured at 2 W. This implies that the sensitivity is deviating from our calibrations before the bead is dragged out of the harmonic region of the optical trap. If correct, a recalibration of the sensitivity could extend the force range at lower laser power.

We base the following recalibration off our observations of the characteristic shape of the nonlinear signal response. In Fig. 2A we obtain a signal (S) vs. stage displacement (x) curve obtained when stretching dsDNA and taken at low laser power (132 mW). A nonlinear response is clearly seen at increasing stage displacement where the signal should remain linear. We then fit a hyperbola to the signal fitting data from the start of the linear regime to the minimum of the the measured signal at (x_m, S_m). The form of the hyperbola fit is as follows:

$$S = a\left(\sqrt{\frac{(x-x_m)^2}{b^2}+1}+\gamma\right), \tag{1}$$

where a, b, x_m and γ are fit parameters. This is repeated at increasing laser power so long as the hyperbolic shape of the nonlinear signal response is clearly observed (i.e, before the overstretching transition). We show the results of these fits in Figs. 2C-E for a, b and γ, respectively. We see that b and γ, which describe the curvature and offset of the nonlinear signal, respectively, remain relatively constant as we vary the laser power and that a, which scales the signal with laser power, increases linearly. Essentially, the shape of the hyperbola is maintained at increasing laser power, it is simply scaled and translated.

Now let us apply this information about the nonlinearity in the signal to recalibrate the 2 W signal we obtained when overstretching dsDNA. When we displace the stage at a constant rate, as the bead begins to move away from the trap center, the curve should become approximately linear and remain so up to 45 pN. However, at 2 W, the signal deviates from linearity prematurely and the resulting force-extension curve reaches the overstretching regime at only ~ 50 pN (see Fig. 3A). To correct for this, we first fit a line between the the points (x_l, S_l) where the linear region begins and (x_n, S_n), where the curve begins to deviate from linearity. We use this fit to identify the stage displacement x^*_{45} where the force should have actually reached the 45 pN upper bound. From the signal recorded between x_l and x^*_{45} (indicated by the shaded regions in Fig. 3), we now fit a hyperbola using Eq. 1.

To constrain this fit we set b, by taking the mean of the values obtained in Fig.2C, and use the linear fit in Fig. 2B to find a. However, the fit is quite sensitive to the location of the minimum of the hyperbola (x_m, S_m), which is determined by x_m and γ. Instead of fixing γ, which is related to S_m by the relation $S_m = a(1+\gamma)$, we instead use a calibration curve, obtained from our low power measurements, for S_m as a function of the initial, "non-stretched" signal S_0 (these points are indicated in Fig. 2A). This calibration curve, Fig. 2E, displays a simple linear relation between S_m and S_0. We use this curve to set γ so that the remaining hyperbolic fit has only one parameter x_m, the location of the minimum, to optimize. The resulting fit to the 2 W data is shown in Fig. 3B.

The hyperbola approximates the observed nonlinearity in the signal response. So long as the actual response of the DNA is linear, the measured signal should roughly follow this hyperbolic fit. We may then correct the signal we measured by directly mapping points along the hyperbola to those along the linear fit. However, the actual response of the DNA only maintains linearity up to ~ 45 pN, and then begins to flatten as it enters the overstretching regime. In this case, to correct the measured signal, the observed photodiode signal is first mapped onto the hyperbolic fit, to account for the nonlinear signal response, which is then mapped onto an extrapolation of the linear portion of the signal response (see Fig. 3B). Note, we only apply this correction for increasing stage displacements until we reach the minimum of the hyperbola at (x_m, S_m). While this choice is somewhat arbitrary, we are only trying to correct for small deviations from linearity in the signal response. At increasing extensions, the bead will eventually get displaced so far from the trap center that we can no longer assume a harmonic restoring force, at which case this rescaling is no longer useful.

If we now use our previously calibrated values for the sensitivity and trap strength, but with the scaled signal, we can recover a more accurate force extension curve. Fig. 3A shows the results of this correction. The force-extension curve obtained at 2 W, after rescaling, now reaches the overstretching regime at a similar force as observed at 3 W. This signature behavior of overstretched DNA acts as a sanity check on our assumptions that went into this rescaling.

B. Peeling of oligomer handles

A common strategy for tethering a protein is to first covalently link the protein to a relatively short ssDNA oligo. This is often accomplished, for example, by linking a thiol group within a free cysteine in the protein to a maleimide-functionalized DNA oligo [11]. Then, in a second step, the oligo is annealed to a longer substrate of dsDNA containing an overhang at one end, and tethered to a glass surface or a bead at the other end. This approach leaves a missing photodiester bond along the DNA backbone, which is referred to as a nick within the DNA. At sufficiently high applied forces, this nick may lead to the oligo handle on the protein dissociating from the rest of the tether. In a rupture force measurement, it is important to design the handle so that it does not rupture before the proteins under study dissociate.

To test the stability of this linkage strategy, we created a series of tethers as described but with the ssDNA oligo directly conjugated to a bead. We varied both the length of the overhang on the substrate and the length of the oligo. Both the glass surface and the bead were attached to the tether by a biotin-streptavidin conjugation, which should be maintained even at the highest forces we apply. We used surface functionalization 2 (hydrophilic w/ BSA-biotin and streptavidin) as described in the Materials and Methods section, as this was the most stable of the methods we explored. This enabled us to study the stability effects of either changing the number of nucleotides in the oligo handle and/or introducing regions of unpaired, ssDNA adjacent to the nick site.

For all the constructs we investigated, the peak in the distribution of rupture forces fell above 45 pN, which is the upper limit to the linear force ramps we can apply with our setup. Throughout, we translated the stage at approximately 50 nm/s for a loading rate of 4.0 ± 0.3 pN/s. This rate was selected as a compromise. While we would be able to capture more of the rupture distribution if we lowered the loading rate, each measurement would then take several minutes or more, which would add significant noise through sample drift. Faster/higher loading rates would shift all the distributions beyond the 45 pN threshold. However, for the different constructs, we could clearly see variations in the tails of the distributions visible below 45 pN (see Fig. 4). In the figure, we indicate all ruptures that occurred at an applied force exceeding 45 pN, but do not show the details of the distribution since the applied force is no longer linear due to the elastic properties of the DNA (this data

is provided in *Supplementary Material*).

Figures 4B and C show the rupture force distributions for 40(OH)-32(OL) and 31(OH)-32(OL), respectively. We use the notation N(OH)-M(OL) to indicate a tether with an N nucleotide overhang (not including the abasic site) conjugated at one end to an M nucleotide long oligo (see Fig. 4A). The same oligo is conjugated to the first 31 nucleotides of the overhang in each construct, but the former has a 9 nucleotide spacer (including the abasic site), whereas the latter has a simple nick. The presence of the spacer shifts the distribution to the right. From Fig. 4G, we see that the fraction of rupture events occurring above our 45 pN range increases from $72 \pm 8\%$ to $84 \pm 3\%$ ($p = 0.0425$, two-sample t-test). Figure 4D is a no nick control where we simply pull on 4.6 kbp biotinylated dsDNA. The ruptures, with this construct, likely occur from the tether pulling away from the surface and provide a measure of the background to our measurements. This control also implies that dissociation by the oligo from the 40(OH)-32(OL) construct is, essentially, negligible.

We note that the 40(OH)-32(OL) construct actually has 32 nucleotides bound to the overhang since we use the same oligo in each measurement and wanted to introduce a nick, with zero spacer, in the 31(OH)-32(OL) construct. Closing the photodiester bond in the 31(OH)-32(OL) construct through an additional ligation step yields similar data to that shown in the no nick control (see *Supplementary Material*). However, our data implies that adding an additional spacer after the oligo, as in the 40(OH)-32(OL) construct, obviates the need for an additional ligation step (at least, at this loading rate), which adds extra time to the protocol and might not be compatible with all protein measurements or experimental conditions.

We next repeated these experiments with a shorter 20 nucleotide oligo (Figs. 4E and F). Here we compared the two constructs 31(OH)-20(OL) and 20(OH)-20(OL). Both utilized the same 20 nucleotide oligo bound to the end of the substrate, but the the former included an 11 nucleotide spacer (including the abasic site), whereas the latter contained only a single basepair gap at the abasic site. Again, the inclusion of a short ssDNA spacer in the sequence significantly increased the stability of the construct. The fraction of ruptures that occur above the 45 pN range jumped from $58 \pm 4\%$ for 20(OH)-20(OL) to $79 \pm 4\%$ for 31(OH)-20(OL) (p=.000903).

A comparison of the data in Fig. 3G shows an increase in stability when we increase the length of the oligo from 20 to 31 bound nucleotides. However, the introduction of an

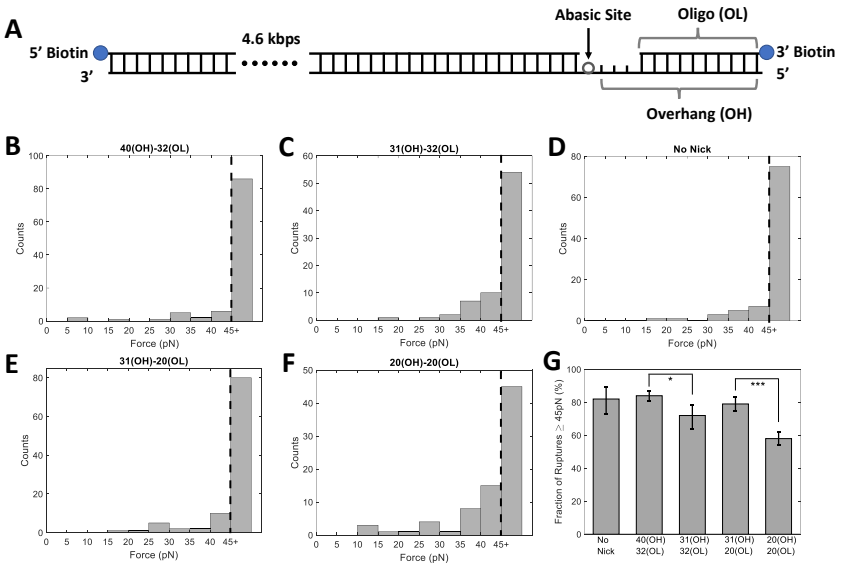

FIG. 4: Rupture force measurements for various oligonucleotide handle attachments. A) Illustration of the DNA tether. At one end of the tether, an abasic site is followed by an overhang (OH) of N nucleotides. A bead attached oligo (OL), M nucleotides in length, is annealed to the end of the overhang. These constructs are indicated as N(OH)-M(OL). B-F) Histograms of the measured rupture forces. All ruptures occurring above 45 pN are indicated by a single bar at 45+ after the dashed line. G) Fraction of ruptures above the 45 pN threshold (error bars indicate $\pm$ std. err.). P-values from a two-sample t-test are indicated as $* < 0.5$ and $*** < 0.001$.

11 nucleotide spacer after the shorter oligo actually provides more stability than increasing the size of the oligo so that 10 additional nucleotides bind to the substrate. In both cases, 40(OH)-32(OL) and 31(OH)-20(OL) , the addition of an ssDNA spacer increases the stability of the tether such that dissociation by the oligo from the construct is, essentially, negligible at this loading rate.

IV. DISCUSSION AND CONCLUSION

In this manuscript, we have systematically extended the range in which rupture force measurements can be performed with axial optical tweezers, up to 45 pN. This is, essentially, the full range that can be accessed when probing the binding of proteins or nucleic acids surface tethered with dsDNA. Within this range of forces the effects of the tether can be accounted for as the mechanics of dsDNA are well described by the eWLC model. The

instrinsic stiffness of dsDNA is captured by the WLC up to $\sim$ 10 pN and then becomes linear until $\sim$ 45 pN. At higher applied forces, dsDNA begins to overstretch with the double-stranded nature of the polymer itself breaking down. This sets an upper limit to the force range within which dsDNA is a useful tether for such measurements.

To reach 45 pN requires a strong axial trap. Since the axial trap stiffness is always much weaker than the lateral trap stiffness this implies high laser powers. We have shown that, with weaker traps, a nonlinear response may be observed within the voltage signal when increasing the applied force. This artifact in the signal results when a trapped bead moves far from the trap center and can lead to an underestimation of the actual force. Fortunately, this nonlinearity can be measured and, to a certain extent, accounted for by rescaling the signal. In our setup, we demonstrated that, by correcting for this nonlinearity in the voltage signal, we could reduce the laser intensity for the optical trap from 3W to 2W, which is a significant reduction in laser power.

At forces approaching 45 pN, careful attention has to be paid to the choice of functional linkages. Antibody-antigen interactions, such as the often employed digoxigenin/anti-digoxigenin pair, will quickly rupture at these forces. We, therefore, only employed much stronger biotin/streptavidin bonds when connecting the dsDNA tether both to the bead and surface. Likewise, we explored several surface functionalization methods. While streptavidin is often deposited on a nitrocellulose coated surface when applying higher forces to dsDNA, we found that simply attaching BSA-biotin to a hydrophilic glass surface was more stable leading to fewer detachments from the surface. Of course, there are covalent methods for linking DNA to a glass coverslip, but these are often complex, expensive, and time-consuming, which motivates a simpler approach.

Finally, we tested the stability of an oligo handle (linked to a bead) that had been annealed to surface tethered DNA. This common method for connecting a protein to a surface tether (in which case the oligo would be covalently linked to a protein) maintains a nick along the template DNA. We found that the insertion of a short ssDNA spacer, just after the region where the oligo binds to the tether, was able to greatly stabilize the binding. A similar result had previously been observed when overstretching dsDNA and observing the breakdown of the DNA duplex [12]. In those experiments, it was found that the energy required to open the DNA duplex increased as an increasing fraction of the dsDNA was converted to ssDNA, which decreased the stiffness of the construct. For our purposes, the

simple introduction of an ssDNA spacer can be used to increase the stability of an oligo, acting as a handle on a protein, bound to the tether. This is much simpler than having to increase the size of the oligo if it's suspected that the oligo is rupturing from the tether before the proteins of interest are unbinding. Adjusting the length of the protein-bound oligo requires covalently linking a new oligo to the protein, which is usually a time consuming and costly process.

Keeping in mind the considerations we have discussed within this manuscript, axial optical tweezers can now be used to explore a much greater range of binding forces and at reduced laser powers. We hope this work will hasten the adoption of axial optical tweezers by the biophysical community, which may serve as a complementary and powerful single-molecule tool for exploring mechanobiology.

V. AUTHOR CONTRIBUTIONS

Z.Z. and J.N.M. designed the research. Z.Z. performed all experiments and analyzed the data. J.N.M and Z.Z. wrote the article.

VI. ACKNOWLEDGMENTS

We wish to thank Emiel Visser, Khadija Lakdawala and Sana Suboh for assistance at various stages of this work. This work was supported by funding from an NSERC Discovery Grant (RGPIN 418251-13).

---

[1] W. N. Sánchez, L. Robeson, V. Carrasco, N. L. Figueroa, F. Burgos-Bravo, C. A. M. Wilson, and N. Casanova-Morales, Quarterly Reviews of Biophysics **55**, e8 (2022).

[2] C. J. Bustamante, Y. R. Chemla, S. Liu, and M. D. Wang, Nature Reviews Methods Primers **1**, 25 (2021).

[3] O. K. Dudko, G. Hummer, and A. Szabo, Proc Natl Acad Sci U S A **105**, 15755 (2008).

[4] E. Evans and K. Ritchie, Biophys. J. **72**, 1541 (1997), ISSN 0006-3495.

[5] S. Yehoshua, R. Pollari, and J. N. Milstein, Biophys. J. **108**, 2759 (2015), ISSN 0006-3495.

[6] J. Lipfert, J. W. J. Kerssemakers, T. Jager, and N. H. Dekker, Nat Methods **7**, 977 (2010).

[7] A. H. Mack, D. J. Schlingman, L. Regan, and S. G. J. Mochrie, Rev Sci Instrum **83**, 103106 (2012).

[8] C. Cecconi, E. A. Shank, S. Marqusee, and C. Bustamante, Methods Mol Biol **749**, 255 (2011).

[9] S. B. Smith, Y. J. Cui, and C. Bustamante, Science **271**, 795 (1996), ISSN 0036-8075.

[10] J. Camunas-Soler, M. Ribezzi-Crivellari, F. Ritort, and K. A. Dill, Annu. Rev. Biophys. **45**, 65 (2016), ISSN 1936-122X.

[11] M. Jahn, A. Rehn, B. Pelz, B. Hellenkamp, K. Richter, M. Rief, J. Buchner, and T. Hugel, Proc Natl Acad Sci U S A **111**, 17881 (2014).

[12] J. van Mameren, P. Gross, G. Farge, P. Hooijman, M. Modesti, M. Falkenberg, G. J. L. Wuite, and E. J. G. Peterman, Proc Natl Acad Sci U S A **106**, 18231 (2009).